Eur J Nucl Med (1986) 12:284–290

European Journal of Nuclear Medicine

A new thresholding method for volume determination by SPECT

L. Mortelmans [1], J. Nuyts [2], G. Van Pamel [1], V. Van den Maegdenbergh [1], M. De Roo [1], and P. Suetens [2]

[1] Department of Nuclear Medicine and [2] ESAT, Department of Electrical Engineering, Katholieke Universiteit, B-3000 Leuven, Belgium

Abstract. The quantification of organ volumes from SPECT images suffers from two major problems: image segmentation and imperfect system transfer function. Image segmentation defines the borders of an organ and allows volume measurements by counting the voxels inside this contour in all slices containing parts of this organ. A review of the literature, showed that several investigators use a fixed threshold (FT) to determine the organ pixels. It is our aim to demonstrate that the threshold has to be adapted to every single case because its value is dependent upon several factors, such as size and contrast. Therefore a threshold selection algorithm, based on the gray level histogram (GLH), is evaluated. It is nearly impossible to calculate and eliminate errors induced by the complex system response function. A correction method based on linear regression is proposed. By minimizing the relative error (σ), a linear correlation ($Y=AX+B$) between the true volume (Y) and the measured volume (X) is established for three fixed thresholds (30%, 40%, 50%) and for the GLH method. The methods are evaluated on a series of nineteen phantoms with a volume range between 9.8 and 202.5 ml. The relative error is minimal for the GLH method. The whole procedure is semi-automated and virtually operator independent.

Key words: Single-photon emission computerized tomography (SPECT) – Quantification – Volume measurements

Quantification is one of the ultimate goals of single-photon emission computerized tomography (SPECT) and can be considered on two levels:

1. measurement of volumes,
2. measurement of absolute radio nuclide concentration, which requires an accurate attenuation correction. The latter cannot be performed at present.

To estimate the volume of an organ from reconstructed SPECT images, two major aspects have to be considered: the segmentation algorithm and the system response.

The purpose of this article is to demonstrate that the fixed threshold method (FT), which is generally used in phantom and clinical studies, has clear short-comings. Hence, we will compare this technique with a more general thresholding algorithm: the gray-level histogram (GLH) method.

1. In a first series of phantom experiments, the dependence of the correct "threshold" upon several factors is demonstrated.
2. Secondly, volume measurements on a series of thyroid phantoms are performed using the two threshold algorithms (FT and GLH).
3. Systematic errors caused by the imperfect system response are reduced by linear regression analysis.

Offprint requests to: L. Mortelmans, M.D., Department of Nuclear Medicine, U.Z. Gasthuisberg, Herestraat 49, B-3000 Leuven, Belgium

Materials and methods

Acquisition and reconstruction

Measurements are carried out with a system (SELO – Italy) consisting of a rotating gantry with two LFOV gamma cameras fitted with general purpose tomographic collimators with long septa. The characteristics of this system have been described previously (Mortelmans et al. 1982). Uniformity correction is performed with the camera in the horizontal position by collecting 30 million counts from a thick, water-filled phantom, homogeneously filled with technetium 99m. Control of pixel size and alignment are performed weekly.

Sixty-four projections, acquired during a continuous rotation of 30 min, are digitized by a DEC computer (PDP 11/34) in a 64×64 matrix with a hardware zoom factor of 1.3. The sensitivity of the system equipped with the high sensitivity collimator is 4,060 counts/sec per μCi per ml for a homogeneously filled cylinder of 20 cm diameter with a rotation diameter of 30 cm.

Thirty-two transaxial slices, two pixels thick, are reconstructed by a filtered back-projection method. The filter used is a raised cosine transition low-pass filter with a -3 dB frequency slightly lower than half the Nyquist frequency (Bellini et al. 1980). After reconstruction, the data are reorganized into frontal and sagittal slices. The size of the elementary voxel is one pixel in the x and y axis (transaxial plane) and two pixels in the z direction (parallel to the axis of rotation). One pixel in zoom mode equals 4.7 mm.

Volume calculation

To obtain the final organ volume, the voxels belonging to the organ are counted and their total is multiplied by

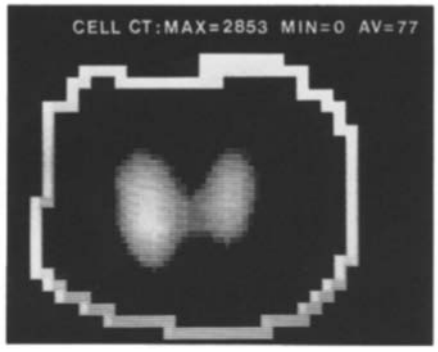

Fig. 1. The GLH method is rather operator-independent. The technologist has only to roughly indicate an ROI which contains the studied organ as demonstrated here for a thryoid study

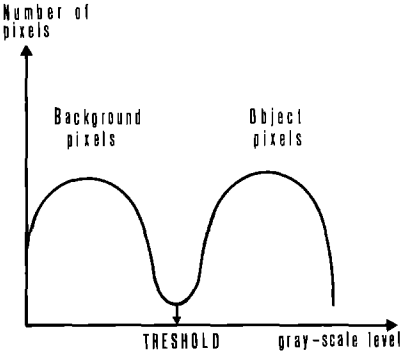

Fig. 2. Principle of gray-level histogram (GLH): the number of pixels (Y-axis) with a certain gray-level (X-axis) are represented. Ideally, a population of background and object pixels can be clearly separated. The separation criterion maximizes the variance σ^2 between the two populations as explained in the text

the elementary voxel size which is determined by phantom measurements.

Segmentation (extraction of the object). Segmentation is performed here with an algorithm which spearates object and background pixels by comparing their intensity with a global threshold: all pixels with an intensity higher than the threshold belong to the object. In the region of interest, roughly defined by the operator so that only the selected organ is included (Fig. 1), the same threshold is used for all the selected slices. The threshold has a fixed value (FT = 30%, 40%, or 50% as commonly used in the literature) or is derived from a gray-level histogram (GLH) (Nobuyuki 1979). This method is briefly described below.

All formula are given for a normalized gray-level histogram: if p_i is the probability of the gray-level i, and L is the number of gray levels, then

$$\sum_{i=1}^{L} p_i = 1. \tag{1}$$

A threshold at gray-level k divides the histogram into two classes: class 0 and class 1. The probabilities of class occurrence are given by

$$\omega_0 = \sum_{i=1}^{k} p_i \quad \text{and} \quad \omega_1 = \sum_{i=k+1}^{L} p_i. \tag{2}$$

The mean class levels are given by

$$\mu_0 = \sum_{i=1}^{k} i p_i/\omega_0 \quad \text{and} \quad \mu_1 = \sum_{i=k+1}^{L} i p_i/\omega_i. \tag{3}$$

The total mean level of the picture is

$$\mu_T = \sum_{i=1}^{L} i p_i. \tag{4}$$

The author presents a set of discriminant criteria to evaluate the "goodness" of the threshold k. It can be proved that all measures presented reach a maximum for the same threshold. The parameter which is the simplest to calculate is the between class variance:

$$\sigma_B^2 = \omega_0(\mu_0 - \mu_T)^2 + \omega_1(\mu_1 - \mu_T)^2 \tag{5}$$

The proposed algorithm evaluates σ_B^2 for all possible gray levels k and selects as a threshold the gray level that maximizes σ_B^2.

In practice, a gray-level histogram of the pixels in the selected ROI in all the slices is constructed (Fig. 2). This histogram contains pixels of two classes: a class of background pixels and a class organ pixels. The algorithm calculates the threshold value which gives the best separation between the two classes as described above. In clinical application, the distinction between the two classes is not as clear as in Fig. 2 either because the valley is not so deep or because there is a clear preponderance of one class without any valley, as indicated Fig. 3 for a thyroid gland.

Correction for the system response function. The correlation between the actual volume (Y) and the computer calculated

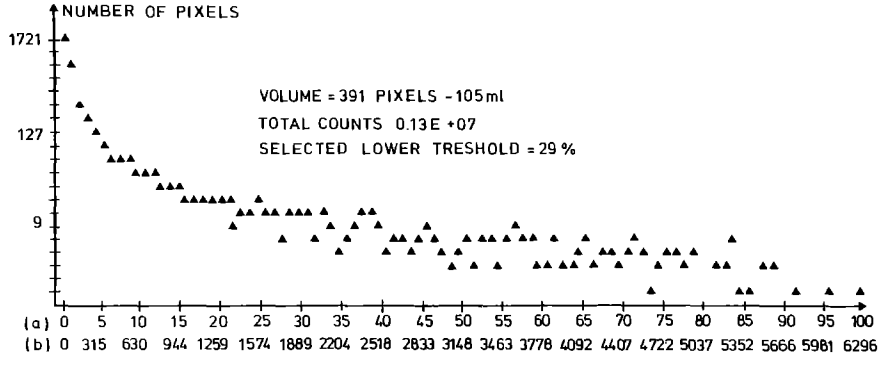

Fig. 3. Gray-level histogram of a thyroid study. On the Y-axis are the number of pixels indicated with the corresponding gray-level on the X-axis (upper row: % of maximum; lower row: absolute counts). Because of the predominance of the background pixels in this clinical situation the separation between the two populations is very vague. (a) = Gray level (% of maximum count density); (b) = counts/pixel

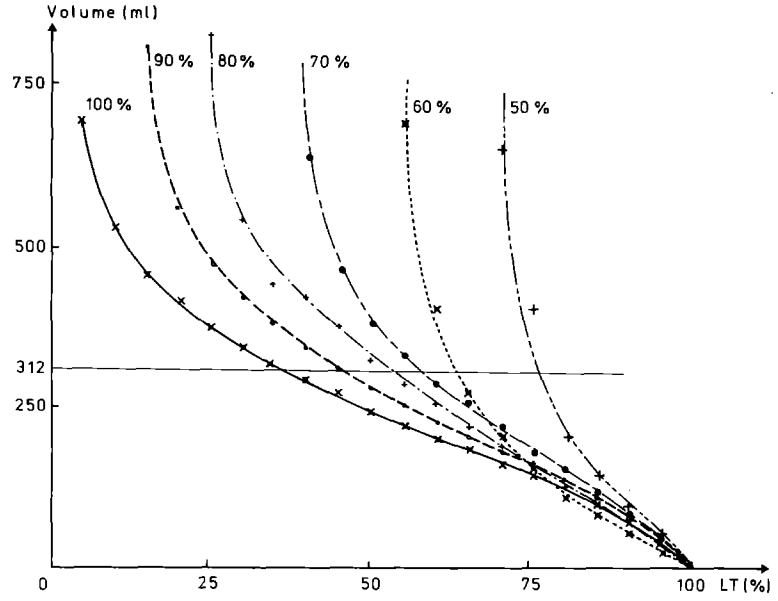

Fig. 4. Influence of the contrast. The correlation between the calculated volume (Y-axis) and the lower threshold (X-axis), used to delineate the bottle with an actual volume of 312 ml, is demonstrated for different contrast. The central bottle, containing 2 μCi/ml, is placed in a cylinder where the tracer concentration is varied to obtain several contrast values

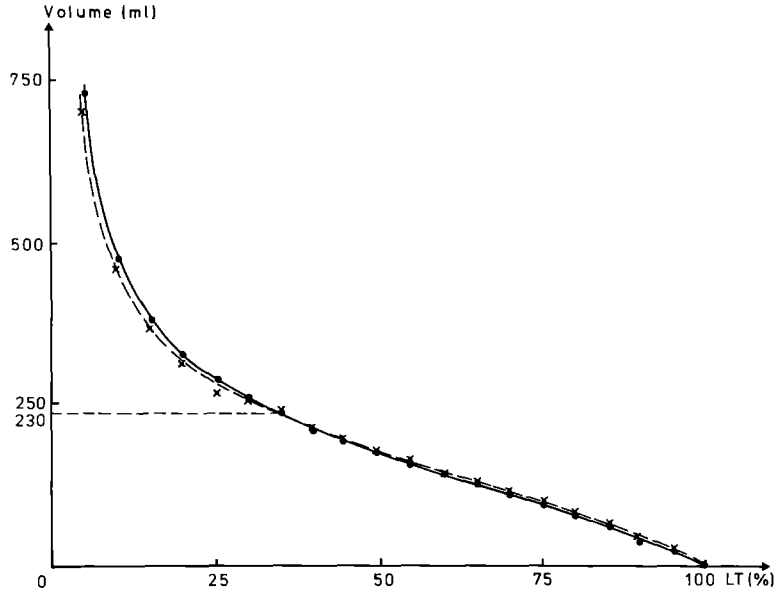

Fig. 5. Influence of attenuation compensation. The same correlation as in Fig. 4 is presented with a central bottle of 230 ml and a contrast of 100%. The volumes are calculated for several thresholds with (full line) and without (dotted line) attenuation correction

volume (X) is defined by a least square linear regression analysis by minimizing the relative error. The correlation is calculated for the transaxial, frontal and sagittal planes.

$$Y = AX + B \tag{6}$$

$$\sigma = \left\{ \left\{ \sum_{i=1}^{n} [Y_i - (AX_i + B)]/X_i \right\}^2 \Big/ (n-2) \right\}^{\frac{1}{2}} \tag{7}$$

n-number of measurements ($n = 19$)

$$X_i = N_i(P_x \cdot P_y \cdot P_z) \tag{8}$$

where N_i = number of voxels, with a count above the selected threshold summed throughout all the slices in a specified spatial orientation. P_x, P_y, P_z is the size of the elementary voxel in the three main directions. Because this size directly influences the final result, a weekly control is performed by phantom measurements.

Phantom studies

1. A small bottle (height = 12.2 cm; diameter = 6.8 cm; volume = 312 ml) was placed in the centre of a perspex cylinder (diameter = 20.5 cm; height = 20 cm). The concentration (Co) of free pertechnetate in the central bottle was 2 μCi/ml; the concentration (Cb) in the background cylinder was varied to change the contrast:

$$(Co - Cb)/Co. \tag{9}$$

For each contrast (100%, 90%, 80%, 70%, 60% and 50%) the volume was calculated for different thresholds (Fig. 4).

2. For a bottle of 229 ml, the volume was calculated for different thresholds after reconstruction with and without attenuation compensation. The attenuation compensation (Bellini et al. 1979) used a body contour obtained by acquisition of Compton scatter and presumed a constant attenuation factor (Fig. 5).

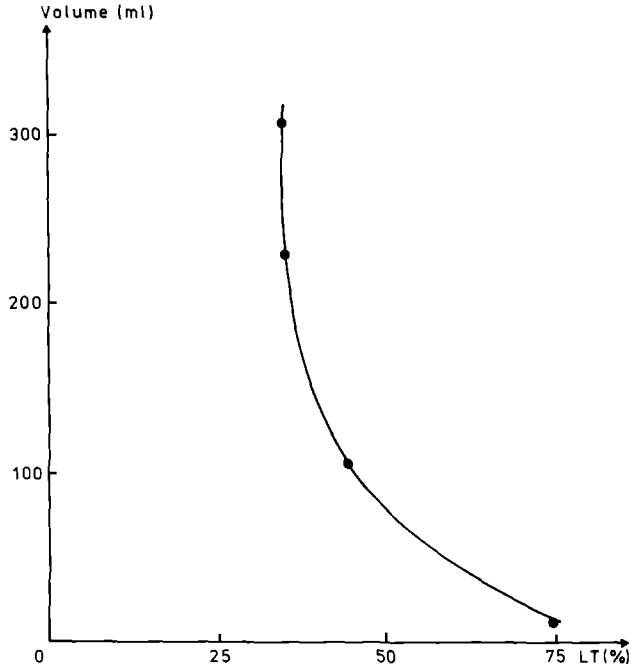

Fig. 6. Influence of the size. The correlation between the actual volume (Y-axis) and the threshold, necessary to obtain the exact volume, is shown

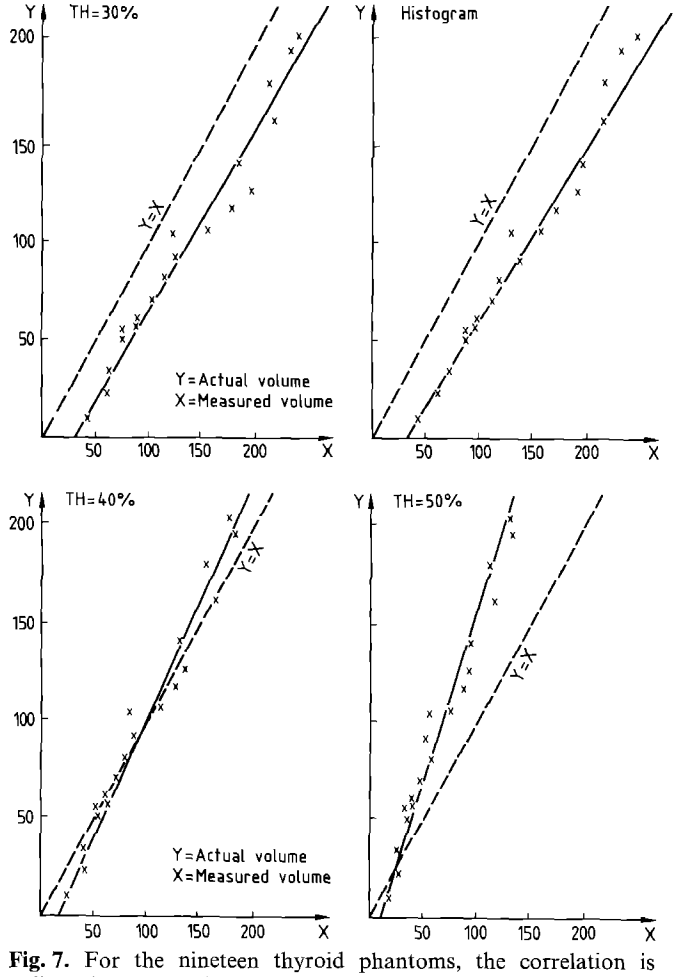

Fig. 7. For the nineteen thyroid phantoms, the correlation is indicated between the actual volume (Y-axis) and the measured volume (X-axis) for three fixed thresholds (30%, 40%, 50%) and the gray-level histogram method. The line obtained by minimizing the relative error is also shown. The volumes are calculated in the transaxial planes

3. In another experiment, bottles with different volumes (11, 121, 229, 312 ml) were placed in the centre of the cylinder. The central bottle contained 2 μCi/ml and the contrast was 100% (the fluid in the cylinder contained no radioactivity). For each bottle the threshold which gave a measured volume equal to the actual volume was determined (Fig. 6).

4. In another experiment, two bottles with their long axes diverging by 20 degrees, to simulate a thyroid gland, were filled with an homogeneous solution of free pertechnetate. Sixty-four projections of nineteen phantoms with varying shape and size (volumes from 9.8 ml to 202.5 ml) were scanned using 30 min continuous rotation (28 s per projection). The measured volume (X) was then calculated by the two methods (FT and GLH) and the correlation with the actual volume (Y) was checked.

Results

1. Figure 4, shows the measured volume of a bottle of 312 ml calculated for different thresholds and contrasts.

2. For a bottle of 229 ml, the volume was calculated for different thresholds after reconstruction with and without attenuation compensation (Fig. 5).

3. Figure 6 demonstrates the influence of the actual volume on the threshold value that gives an exact calculation of the actual volume.

4. The volumes of all the thyroid phantoms, calculated in the transaxial plane, were compared with the true volumes for three fixed thresholds (30%, 40%, 50%) and for the GLH method (Fig. 7). Routinely, the same calculations were also performed in the frontal and sagittal planes. This is illustrated (Fig. 8) for the GLH and the FT=30%. The parameters of the linear regression and the relative error are summarized in Table 1 for the four thresholds and the three reconstruction planes. The influence of the size of the ROI and the number of slices selected on the calculated volume is shown in Table 2.

Discussion

As stated by many authors, functional or afunctional volume measurements offer a great potential in every day nuclear medicine. A variety of clinical applications have already been described: quantification of viable or nonviable myocardium (Caldwell et al. 1982, 1984; Kirsch et al. 1981; Keyes et al. 1981), liver and spleen volume measurements (Strauss and Clarius 1984; Kan and Hopkins 1979), kidney volume measurements (Tauxe et al. 1982), thyroid volume (Saphiro et al. 1980), local cerebral blood volume (Kuhl et al. 1980). Some authors have stated that even measurements of absolute concentration are possible with homogeneously filled phantoms (Jaszczak et al. 1981; Axelson et al. 1982; Pupi et al. 1983).

Several factors may influence the quantitative reliability of SPECT:

1) the reconstruction algorithm with the chosen filter,
2) the angular and linear spatial sampling,
3) the limited number of events,

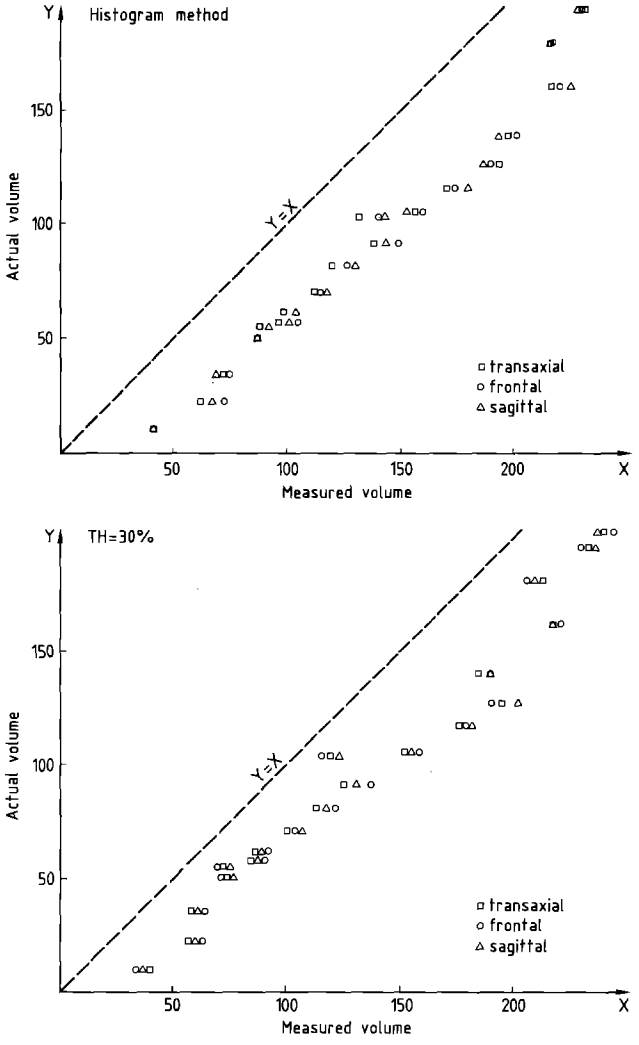

Fig. 8. For the GLH method and a fixed threshold = 30%, the correlation is shown between the measured volumes (X-axis) in the three main section planes and the actual volume (Y-axis). The line of identity is also indicated

Table 1. Linear regression ($Y = AX + B$) between actual volume (Y) vs measured volume (x) by minimizing the relative error (σ)

Section plane	Histogram	Th = 30%	Th = 40%	Th = 50%
Transaxial				
A	0.87	0.91	1.23	1.78
B	−27.5	−24.5	−20.7	−20.9
σ	8.4%	13.3%	15.5%	17.7%
Frontal				
A	0.83	0.87	1.23	1.71
B	−26.4	−22.6	−24.0	−20.0
σ	15.8%	15.9%	17.2%	18.1%
Sagittal				
A	0.84	0.86	1.21	1.66
B	−26.6	−21.6	−21.9	−18.4
σ	11.0%	14.6%	16.7%	20.9%

Table 2. Operator independence of the GLH method

A) Influence of the size of the ROI (S1 < S2)
(S = number of pixels in the ROI)

	S1	M1	C1	S2	M2	C2
Transaxial	754	125	81.7	2,465	129	85.2
Frontal	1,017	130	86.1	2,956	137	92.2
Sagittal	602	131	87	3,379	140	94.8

B) Influence of the number of slices (N1 < N2)

	N1	M1	C1	N2	M2	C2
Transaxial	13	121	78.3	25	131	87
Frontal	7	118	75.7	19	121	78.3
Sagittal	12	120	77.4	26	124	80.9

Note: M = measured volume; C = corrected volume; Actual volume = 80.6 ml

4) the attenuation and the scattering of the gamma photons,

5) the segmentation method used to extract the object of interest from the image,

6) the performance of the gamma camera, collimator and computer. The first two parameters are similar for all commercial systems presently available. Factor three is inherent to nuclear medicine procedures. The volumes calculated in our phantom studies are very similar with an without attenuation compensation (Fig. 5). In clinical practice the problem of attenuation is more complex because of variable attenuation due to tissue of different densities. Until now, all commercial software uses a constant attenuation factor. Only a few methods, with varying success, have been suggested for correction of scatter. The segmentation problem is usually solved by one of the following three approaches: thresholding, edge detection or region growing.

a) *Thresholding algorithms* presume that background and object have a sufficiently different gray-level distribution. In order to extract the object pixels from the background, their intensity is compared with a threshold. The major problem here is the selection of the threshold. Normally global thresholding is used: i.e. the same threshold is used for the entire image. The threshold is chosen independently of the image, or is derived from some gray-level histogram. More complex algorithms use a local threshold, which is automatically adapted to local changes in the gray-level distribution.

b) *Edge detection algorithms* presume that background and object are separated by abrupt changes in gray level value (high gradients). A large amount of edge detection filters has been invented. One class of algorithms starts by converting the entire image to a gradient, or edge, image, using a filter or set of filters. In a second step they try to extract and link boundary pixels and to eliminate edges caused by noise. This second step usually involves a series of processing steps, such as thresholding, erosion, dilatation, etc. Another class operates on the original gray-level image, and tries to find and track the contour of the object.

c) *Region growing methods* start with partitioning of the image into small regions. Each region is characterized by one or more features. Next, the features of neighbouring regions are compared. If they are not significantly different the regions are merged. This process is repeated until all remaining areas differ.

Split and merge is an extension of region growing: inho-

mogeneous regions of the image are split into smaller regions, and regions with similar features are merged. The procedure is repeated until the image is partioned into a set of internally homogeneous regions, significantly different from their neighbours.

In general, edge detecting algorithms are more powerful and more computation intensive than thresholding algorithms. The complexity and power of region growing depend highly on the chosen feature set. Region growing is usually computation intensive since a lot of iterations may be required to find the desired regions.

The nature of SPECT images makes them suitable for the three classes of segmentation. To avoid a computation intensive algorithm in clinical practice, two global thresholding algorithms are compared: an image independent fixed threshold and a thresholding algorithm which is based on a gray-level histogram (Nobuyuki 1979).

Most authors use a fixed threshold in clinical and phantom measurements. Kawanura et al. (1984) have found the best correlation between measured and actual volumes of kidney phantoms with a threshold of 51% and Tauxe (1982) mentions a threshold of 46% for elliptical phantoms of more than one l and 45% for phantoms smaller than one l and with this threshold value he has found a good correlation with ultrasound in DMSA kidney studies (Tauxe et al. 1983). For the calculation of infarct size, a threshold of 50% of the maximum count within the entire ventricle (Wolfe et al. 1985) is used in the case of thallium SPECT studies and a threshold of 65% is used in the case of SPECT pyrophosphate studies (Corbet et al. 1984). For left ventricular volume determination with gated SPECT, a threshold value of 43% yielded the best correlation with count-based plasma techniques (Underwood et al. 1985).

The fact that only one threshold value gives the exact volume in a particular combination of tracer distribution, imaging device and reconstruction software, argues against a fixed threshold without any additional correction. Even with the same collimator-computer-software combination, the exact threshold is influenced by the size and the contrast of the lesions (Soderborg et al. 1982). As demonstrated here, a higher threshold is needed for lower contrast (Fig. 4) and a smaller size (Fig. 6).

The study of thyroid phantoms (experiment 4) reveal a systematic error in the volume calculation for both methods: in the transaxial plane there is an overestimation of the actual volume for all phantoms with the histogram method and a fixed threshold of 30%. For a threshold of 40% or 50% we found an overestimation of the smallest volumes and an underestimation of the largest volumes (Fig. 7). As is shown in Fig. 8 for the GLH method and a fixed threshold of 30%, roughly the same error is found for volume calculations in the three section planes.

This systematic error can probably be explained by the response function of the system. Because of its complexity and nonlinearity, it is impossible to define all system induced errors. The effect of this systematic error is estimated by a least square linear regression analysis ($Y = AX + B$) between the actual volume (Y) and the calculated volume (X) by minimizing the relative error. The calculated values A and B and the relative error for the transaxial, frontal and sagittal planes are shown in Table 1 and the regression lines are shown in Fig. 7. The dependence of the systematic error on other parameters such as contrast and object shape is not yet evaluated. The relative error is minimal for the

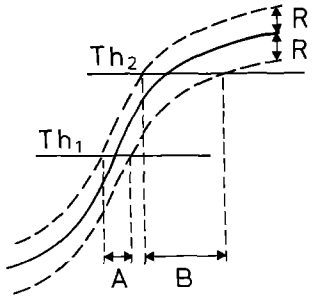

Fig. 9. The straight line represents the profile through to border of an organ. The dashed lines represent the noise limits. A lower value of the threshold (Th1) cuts the profile on a steeper part where the noise influence (A) is smaller than in the case of a higher lower threshold (Th2) with a more pronounced noise influence (B)

GLH method (8.47% in the transaxial plane). The relative error is larger for the fixed threshold and increases with the threshold value. This can be explained by the fact that the higher thresholds of 40% and 50% define an edge that cuts the objects profile in a region of lower edge gradients where the noise has a greater influence than in the region of steeper gradients defined by a lower threshold values (Fig. 9). For the same method, the relative error was minimal in the transaxial planes, followed by the sagittal planes and, finally, the frontal planes. This is explained by the fact that the transaxial planes are nearly perpendicular to the long axis of the phantom so that transaxial slices are smaller than sagittal slices which, in turn, are smaller than frontal slices: the partial volume effect will play a smaller role in the transverse slices. On the other hand, the transaxial slices are reconstructed on a 64×64 pixel matrix and the sagittal and frontal slices in 64×32 matrix because the slices are two pixels thick. Because of the moderate resolution of a rotating gamma camera system (almost 20 mm for a rotation diameter of 40 cm), the theoretical lower measurement limit is approximately 8 ml. We were able to calculate a thyroid volume of 9.7 ml.

The GLH method has the advantage of being (semi-) automatic. The operator has only to roughly define an ROI which contains the studied organ. As indicated in Table 2, the size of the ROI and an overestimation of the number of slices only slightly influence the final result.

Because of the assumption of two pixel clones, hypoactive zones of an organ are counted as background pixels and are as such not added to the organ volume. Before using an algorithm, we must decide whether the available information answers the clinical question. Because of the need for evaluation in a clinical environment, we applied these volume measurements to calculate the radioactive dose required for hyperthyroid patients, spleen volumes (hypersplenisme), kidney volumes (influence of treatment on DMSA studies), and volume of viable myocardium (T1.201), etc.

It is concluded that the GLH method adapted to various conditions of use by regression analysis is a simple, semi-automatic, fast method that estimates a functional volume by SPECT with a relative error of about 8%, which is definitely smaller than the more widespread fixed threshold technique. Clinical evaluation and comparison with more sophisticated edge detection algorithms are still required.

Acknowledgements. We thank Mrs. M.J. Vangoetsenhoven for her skilled secretarial assistance and Mrs. K. De Backer and Mr. R. Maris for the laborious execution of the phantom measurements.

References

Axelsson B, Israelson A, Larson S, Msaki P (1982) Attenuation and scatter correction aiming at quantitative SPECT. Proceedings of the third world congress of nuclear medicine and biology, vol I:514–517

Bellini S, Piacentini M, Caffosio C, Rocca F (1979) Compensation of tissue absorption in emission tomography. IEEE Trans ASSP-27, 3:213–218

Bellini S, Caffosio C, Piacentini M, Rocca F (1980) Design of a computerized emission tomographic system. In: Cappellini V, Costantinides A (eds). Digital signal processing. Academic Press, New York, pp 207–216

Caldwell JH, Williams DL, Hamilton CW, Ritchie JL, Harp GD, Eisner RL, Gulberg GT, Nowak DJ (1982) Regional distribution of myocardial blood flow measured by single photon emission tomography: comparison with in vivo counting. J Nucl Med 23:490–495

Caldwell JH, Williams DL, Harp GD, Stratton JR, Ritchie JL (1984) Quantitation of size of relative myocardial perfusion defect by single photon emission computed tomography. Circulation 70, 6:1048–1056

Corbett JR, Lewis SE, Wolfe CL (1984) Measurement of myocardial infarct size by technetium pyrophosphate single-photon tomography. Am J Cardiol 54:1231–1236

Jaszczak RJ, Coleman RE, Whitehead FR (1981) Physical factors affecting quantitative measurements using camera based single photon emission computed tomography (SPECT). IEEE Trans Nucl Sci NS-28:69–80

Kan MK, Hopkins BG (1979) Measurement of liver volume by emission computed tomography. J Nucl Med 20:514–520

Kawamura J, Itoh H, Yoshida O, Fujita T, Torizuka K (1984) In vivo estimation of renal volume using a rotating gamma camera for 99mTc-dimercaptosuccinic acid renal imaging. Eur J Nucl Med 9:168–172

Keyes JW, Brady TJ, Leonard PF, Svetkoff DB, Winter SM, Rogers LW, Rose EA (1981) Calculation of viable and infarcted myocaridal mass from Thallium-201 tomograms. J Nucl Med 22:339–343

Kirsch CM, Darsee JR, Hill TC, Holman BL (1981) In vivo assesment of infarct size in dogs using a transaxial single photon emission computed tomography system. J Nucl Med 22:P53

Kuhl DE, Alavi A, Hoffman E (1980) Local cerebral blood volume in head-injured patients. J Neurosurg 52:309–320

Mortelmans L (1982) Single photon emission computerized tomography: a new dimension in nuclear medicine – system characterization. J Belge Radiol 65:445–463

Nobuyuki O (1979) A threshold selection method from gray-level histograms. IEEE Trans Syst, Men Cybern SMC-9:

Pupi A, Formioconi A, Bisi G, Alcidi L, La Cava G, Voegelel R (1983) J Nucl Med 24:93

Saphiro B, Rigly L, Britton KE (1980) The assessment of thyroid volume with single photon emission tomography. Nucl Med Commun 1:33–36

Soderborg B, Dahlom M, Kalkberg N, Virgin J (1982) Numerical analysis of ECT. Proceedings of the third world congress of nuclear medicine and biology, vol I:514–517

Strauss LG, Clarius JN (1984) Single photon emission computerized tomography (SPECT) for estimate of liver and spleen volume. J Nucl Med 25:81–85

Tauxe WN, Sousaline FR, Todd-Poktopek AE (1982) Determination of organ volume by single photon emission tomography. J Nucl Med 23:984–987

Tauxe WN, Todd-Pokropek A, Soussolise F (1983) Estimates of kidney volume by single photon emission tomography: a preliminary report. Eur J Nucl Med 8:72–74

Underwood SR, Walton S, Laming RL (1985) Left ventricular volume and ejection fraction determined by gated blood pool emission tomography. Br Heart J 53:216–222

Wolfe CL, James DF, Corbett JR (1985) Determination of left ventricular mass using single-photon emission computed tomography. Am J Cardiol 56:761–764

Received September 21, 1985 / April 26, 1986